T CELLS

High-throughput peptide-MHC complex generation and kinetic screenings of TCRs with peptide-receptive HLA-A*02:01 molecules

Andreas Moritz[1,2]*, Raghavendra Anjanappa[3], Claudia Wagner[2], Sebastian Bunk[2], Martin Hofmann[2], Gabriele Pszolla[2], Ankur Saikia[3], Maria Garcia-Alai[4], Rob Meijers[4], Hans-Georg Rammensee[1], Sebastian Springer[3], Dominik Maurer[2]*

Major histocompatibility complex (MHC) class I molecules present short peptide ligands on the cell surface for interrogation by cytotoxic CD8^{+} T cells. MHC class I complexes presenting tumor-associated peptides such as neo-antigens represent key targets of cancer immunotherapy approaches currently in development, making them important for efficacy and safety screenings. Without peptide ligand, MHC class I complexes are unstable and decay quickly, making the production of soluble monomers for analytical purposes labor intensive. We have developed a disulfide-stabilized HLA-A*02:01 molecule that is stable without peptide but can form peptide-MHC complexes (pMHCs) with ligands of choice in a one-step loading procedure. We illustrate the similarity between the engineered mutant and the wild-type molecule with respect to affinity of wild-type or affinity-matured T cell receptors (TCRs) and present a crystal structure corroborating the binding kinetics measurements. In addition, we demonstrate a high-throughput binding kinetics measurement platform to analyze the binding characteristics of bispecific TCR (bsTCR) molecules against diverse pMHC libraries produced with the disulfide-stabilized HLA-A*02:01 molecule. We show that bsTCR affinities for pMHCs are indicative of in vitro function and generate a bsTCR binding motif to identify potential off-target interactions in the human proteome. These findings showcase the potential of the platform and the engineered HLA-A*02:01 molecule in the emerging field of pMHC-targeting biologics.

INTRODUCTION

Presentation of peptides on cell surface major histocompatibility complex (MHC) molecules plays a fundamental role for the immune response against viral infection or cancer (1). MHC class I molecules are trimeric complexes that consist of a polymorphic heavy chain, the light chain β2-microglobulin (β2m) and a peptide ligand, typically between 8 and 10 amino acids long and derived from cellular proteins by degradation. T cells can recognize specific peptide-MHC complexes (pMHCs) with their T cell receptor (TCR) and initiate an immune response. Soluble pMHCs were first generated using protein expression and refolding techniques in 1992 and have since found use for many immunological research applications, e.g., identification of antigen-specific T cells through flow cytometry or affinity measurements of pMHC-TCR interactions (2–5).

The binding affinity of TCRs for their cognate pMHC has a substantial impact on the functionality of T cells (6). Thus, efforts have been made to increase the affinity of TCRs for clinical applications (7). Extensive maturation experiments have produced TCRs with picomolar affinities, a range typically found only in antibodies. They bind specific pMHCs with a long interaction half-life and have attracted attention as the tumor cell engaging component in bispecific T cell engager formats (8, 9).

A potential downside of TCR binding affinity enhancement is the introduction of off-target toxicities. These can occur by unintentionally increasing the affinity toward other pMHCs in parallel to the target, due to the inherent cross-reactivity of TCRs (10). Multiple cases of cross-reactivity have been reported in clinical studies (11–13). Comprehensive screening is therefore necessary to ensure not only efficacy but also specificity and safety of therapeutic candidates (14). This is a task of high complexity given the currently established size of the immunopeptidome, with at least 150,000 MHC class I ligand peptides identified by mass spectrometry (15).

We here present a disulfide-stabilized and peptide-receptive human leukocyte antigen (HLA)–A*02:01 molecule (DS-A*02:01) that can be produced as a functionally empty molecule and forms pMHCs in a simple one-step peptide loading procedure, allowing high-throughput pMHC generation. We show that pMHCs generated using this modified MHC molecule are comparable to the wild-type MHC molecule with respect to their interactions with TCRs. We also describe a high-throughput pMHC–bispecific TCR (bsTCR) binding kinetics measurement platform that uses DS-A*02:01 to generate large libraries of pMHCs for screening against affinity-enhanced bsTCRs. We generate a comprehensive pMHC-bsTCR binding motif with this platform and use it to identify potential off-target pMHC interactions.

RESULTS

Design and production of DS-A*02:01 molecules

Molecular dynamics simulations of empty and peptide-loaded MHC class I molecules have indicated an increased mobility in the F-pocket, the region that typically accommodates the C terminus of peptide

[1]Department of Immunology, Institute for Cell Biology, University of Tübingen, Tübingen, Germany. [2]Immatics Biotechnologies GmbH, Tübingen, Germany. [3]Department of Life Sciences and Chemistry, Jacobs University, Bremen, Germany. [4]European Molecular Biology Laboratory (EMBL), Hamburg Outstation, Notkestrasse 85, D-22607 Hamburg, Germany.
*Corresponding author. Email: andreas.moritz@student.uni-tuebingen.de (A.M.); maurer@immatics.com (D.M.)

ligands, in absence of bound peptide (*16*). In previous studies with the mouse MHC class I molecule H-2K[b], the introduction of a disulfide bond between opposing residues in the F-pocket, by mutating a tyrosine at position 84 and an alanine at position 139 to cysteines, resulted in the stabilization of the complex. The mutant could be refolded as an empty MHC molecule and was capable of binding peptide ligands (*17*, *18*).

We hypothesized that the same concept could be applied to the human MHC class I molecule HLA-A*02:01. The modifications were introduced into an HLA-A*02:01 heavy chain expression plasmid, produced as inclusion bodies in *Escherichia coli*, and incubated with similarly produced β_2m and the dipeptide H-Gly-Met-OH (GM) (Fig. 1A). This dipeptide has a very low affinity for the MHC class I complex and assists the refolding (*19*). During size exclusion chromatography (SEC), the dipeptide dissociates quickly from the binding pocket by buffer exchange against the running buffer, yielding purified and presumably empty DS-A*02:01.

Although the absence of the dipeptide in the final product could not be confirmed directly because of its small size, indirect evidence supports the assumption that the peptide binding pocket of the disulfide-stabilized molecule is empty. Thermal stability analysis of the DS-A*02:01 molecule with and without dipeptide removal through buffer exchange revealed a lower melting temperature of the former, supporting the hypothesis that the complex-stabilizing dipeptide had dissociated (*20*). Wild-type HLA-A*02:01 complexes (WT-A*02:01) can also be produced with the dipeptide but denature when attempting to remove the dipeptide by buffer exchange. Together, these observations demonstrate that DS-A*02:01 can be produced in a stable and presumably empty state through the introduction of the disulfide bond.

Analyzing binding kinetics using soluble TCRs and wild-type or disulfide-stabilized MHCs

Next, we investigated whether the presumably empty HLA molecule could also be regarded as functionally empty, specifically whether the molecule was capable of pMHC formation and TCR ligand binding. Binding kinetics measurements were performed by biolayer interferometry on an Octet RED384 using the refolded TCR 1G4 as soluble analyte. This TCR recognizes the HLA-A*02:01–specific peptide SLLMWITQC (ESO 9C) derived from the cancer testis antigen NY-ESO-1 or its synthetic variant SLLMWITQV (ESO 9V) (*21*, *22*). Biotinylated DS-A*02:01 was immobilized on streptavidin-coated biosensors, either directly in its empty state or after 5 min of incubation with the peptide ESO 9V (Fig. 1B). Kinetics were measured across multiple 1G4 concentrations and WT-A*02:01 directly refolded with ESO 9V served as control.

1G4 TCR binding to either DS-A*02:01 ESO 9V or WT-A*02:01 ESO 9V was very similar with respect to sensorgrams and dissociation constants (K_d) identified by curve fittings, indicating successful peptide loading and no interference of the disulfide bridge with TCR binding (Fig. 2, A and B). A weak binding signal (but no dissociation) could be detected for the functionally empty immobilized DS-A*02:01 monomer at high concentrations of 1G4 (Fig. 2C), which was not observed when loaded with peptide not recognized by 1G4, such as SLYNTVATL (Fig. 2D). The weak signal obtained with functionally empty DS-A*02:01 might be explained by nonspecific interactions of the TCR at high concentrations with the empty binding pocket, a state that is typically not encountered by TCRs in vivo. Other A*02:01-restricted soluble TCRs with varying specificities behaved similarly, showing no binding to irrelevantly loaded DS-A*02:01
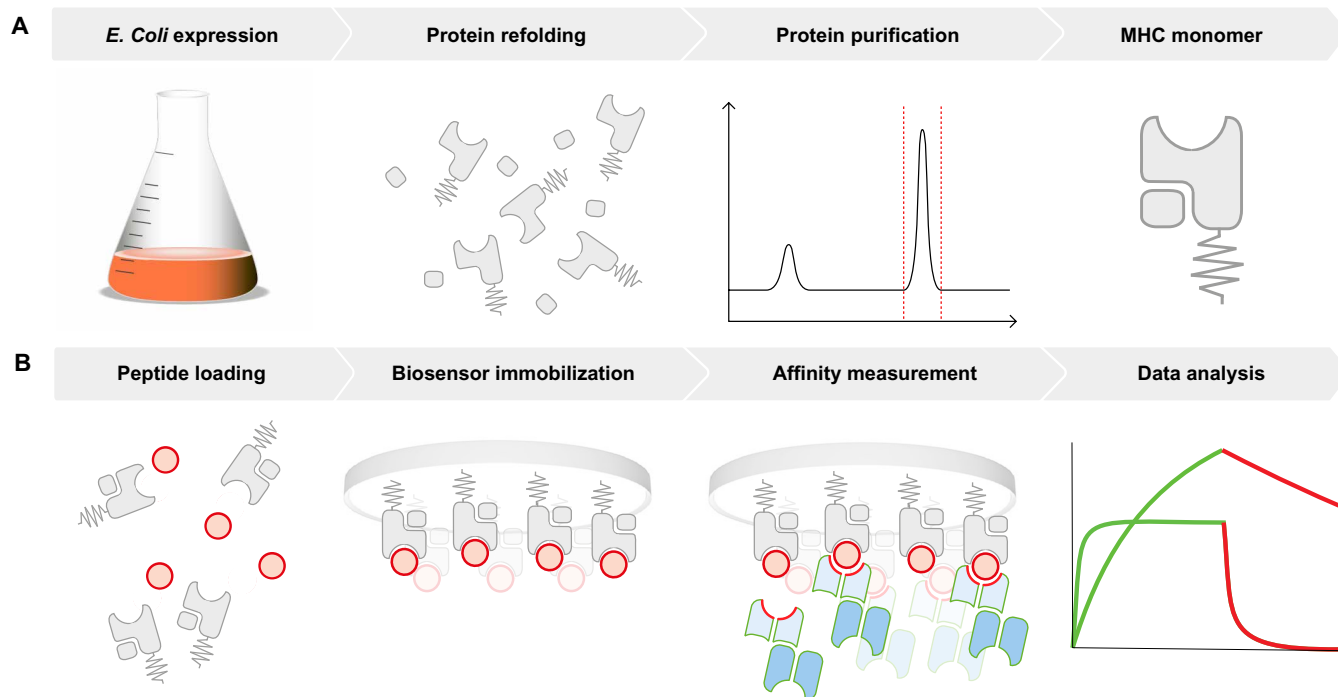
Fig. 1. Overview of DS-A*02:01 production and usage for affinity measurements. (**A**) Expression plasmids of heavy chain and β_2m are transfected into *E. coli* and proteins of interest expressed in inclusion bodies. HLA monomers are purified using size exclusion. (**B**) Functionally empty DS-A*02:01 molecules can be loaded with peptide ligands by incubation at room temperature. For affinity measurements, they can be immobilized on functionalized biosensors, e.g., by biotin streptavidin interaction, and used to record association and dissociation of TCRs or TCR-like molecules.
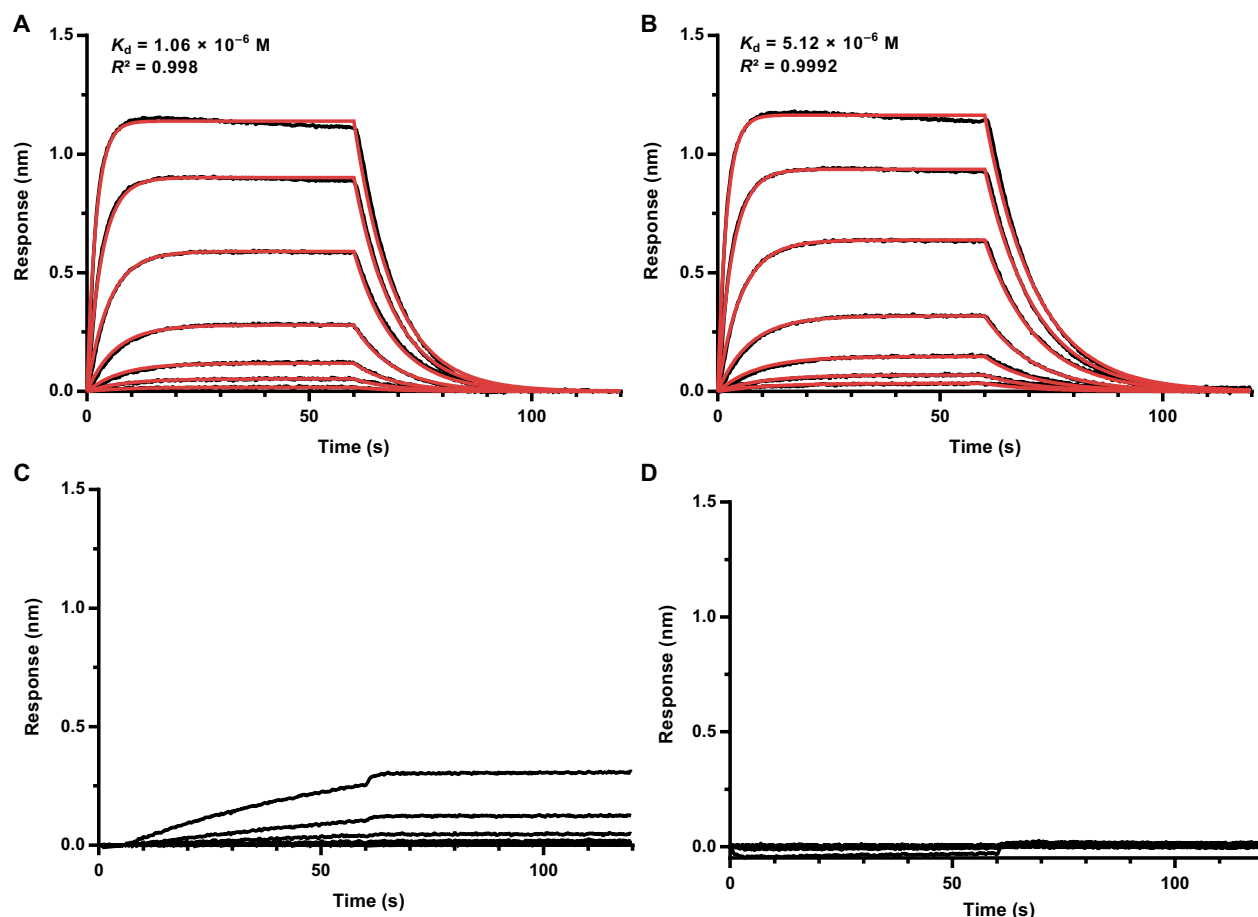
Fig. 2. Association and dissociation behavior of 1G4 TCR with different pMHCs. Raw data are displayed in black and curve fittings are in red. All measurements performed as 1:2 analyte dilution series starting at 24 μM. (**A**) Binding curve of the 1G4 TCR against immobilized DS-A*02:01 ESO 9V pMHC. (**B**) Binding curve of the 1G4 TCR against immobilized WT-A*02:01 ESO 9V pMHC. (**C**) Binding curve of the 1G4 TCR against immobilized empty DS-A*02:01. (**D**) Binding curve of the 1G4 TCR against immobilized DS-A*02:01 SL9 pMHC.

pMHCs but association to functionally empty molecules, albeit but with a rela.tively lower response (fig. S1). DS-A*02:01 can be stored for a least a year at −80°C, and no degradation or impaired peptide receptiveness could be detected compared with fresh preparations (fig. S2).

Crystal structure of the 1G4 DS-A*02:01 ESO 9V TCR-pMHC complex

To further confirm that the 1G4 TCR recognizes DS-A*02:01 ESO 9V indistinguishably from WT-A*02:01 ESO 9V, TCR and disulfide-stabilized MHC refolded with ESO 9V were cocrystallized, as reported previously for the WT HLA-A*02:01 ESO 9V molecule and analyzed by x-ray crystallography (table S1) (*22*). Comparison of the crystal structures revealed a high degree of structural overlap between both complexes. The backbone of both HLA-A*02:01 molecules aligned almost perfectly with a root mean square deviation (RMSD) value of 1.14 Å calculated over Cα (constant portion of the α chain of a T cell receptor; Fig. 3A). The same was true for both bound peptides including their side chains with an RMSD value of 1.27 Å calculated over all atoms, even when in close vicinity to the disulfide bond (Fig. 3B).

Similar conclusions could be made for the interaction with the 1G4 TCR. The complementarity-determining region (CDR) loop

regions interacting with the peptide and the MHC backbone did show slight deviations of the interface and a small change in the docking angle of 4.13°, when comparing the 1G4/WT-A*02:01/ESO 9V and the 1G4/DS-A*02:01/ESO 9V crystal structures. This shift was still within the range of expected deviations for the same complex when crystallized repeatedly (Fig. 3, C and D). Together, determined binding affinities and crystal structure showcase peptide receptiveness and similar properties of the DS-A*02:01 pMHCs compared with wild-type complexes with respect to TCR binding.

TCR binding affinities to peptide libraries displayed using wild-type or disulfide-stabilized MHCs

Having established the application of the DS-A*02:01 molecule as ligand equivalent to WT-A*02:01 for unmodified TCRs, we wanted to expand this analysis toward mutated high-affinity TCRs and a larger number of peptide ligands. To this end, we used the bsTCR bs-868Z11-CD3 as a second analyte. This molecule is composed of the single-chain TCR (scTv) 868Z11, an affinity-matured TCR recognizing the HIV p17 Gag (77 to 85) derived and HLA-A*02:01–presented peptide SLYNTVATL (SL9) with antibody-like affinity, linked to a humanized anti-CD3 antibody functioning as T cell–engaging domain (fig. S3) (*8, 23, 24*).
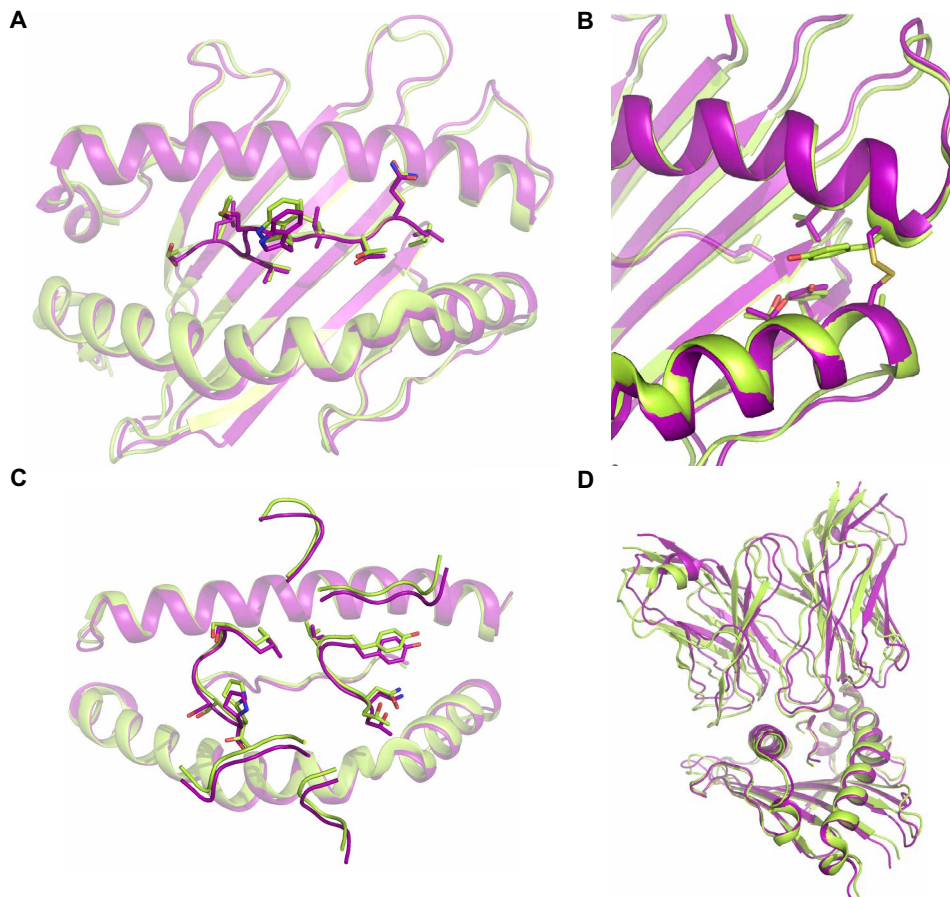
Fig. 3. Crystal structure of DS-A*02:01 ESO 9V and WT-A*02:01 ESO 9V in complex with 1G4. (**A**) Overlay of WT and DS-A*02:01 structure with focus on peptide and amino acid side-chain orientation. (**B**) Close-up of the F-pocket and the introduced disulfide bond between α_1 and α_2. (**C**) Overlay of the 1G4 CDR loops interacting with the peptide and the MHC backbone. (**D**) Overlay of both crystal structures from a lateral perspective.

ligands resulted in a wide range of different pMHC-bsTCR binding affinities, ranging from undetectable within the sensitivity range to equally strong compared with the interaction with the SL9 pMHC.

For direct comparison, all measured pMHCs were selected that had evaluable curves at both analyte concentrations and curve fitting results accompanied by coefficient of determination (R^2) values of at least 0.9. K_d values for the resulting 140 peptide ligands correlated well across the whole range (Fig. 4D). Discrepancies were within 2-fold range for more than 90% of the pMHC pairs and 6.82-fold differences at most. Within the group with higher than twofold changes, a trend toward a larger dissociation constant for measurements with the DS-A*02:01 molecule was observed. The amount of functional pMHC immobilized on each biosensor expressed by the reported R_{max} value was comparable for both wild-type and disulfide-stabilized pMHCs (fig. S4).

High-throughput pMHC-bsTCR kinetics screenings for binding motif generation

Quick and flexible generation of pMHCs is a key requirement to facilitate the collection of large binding affinity datasets against many different pMHCs. One example of such a dataset is screening of a positional scanning library to generate a pMHC-bsTCR binding motif, which can serve as one component in a bsTCR safety screening approach. To perform such measurements, the pMHC should ideally be used as a soluble analyte because this offers multiple advantages. First, immobilizing the same ligand with known activity repeatedly, for example, a bsTCR, allows better interpretation of the fitting results, especially the reported R_{max} value. Second, it enables quicker and much more cost-effective high-throughput screenings, because a broad variety of regenerable biosensors capable of repeatedly immobilizing bsTCRs exist. Third, immobilizing the bsTCR is the only orientation available for measuring monovalent affinity when a bsTCR or antibody has multiple pMHC binding moieties, because, with immobilized pMHCs, only avidity can be measured.

Although the UV-mediated peptide ligand exchange offers similar throughput, its exchange efficiency is dependent on rapid complex stabilization by the new peptide during the UV exposure. Lower-affinity peptides, in particular, can fail to do so, resulting in a decreased functional pMHC concentration after the exchange, which can be detected using an anti-β_2m enzyme-linked immunosorbent assay (fig. S5A). This makes UV exchange a less reliable tool to produce pMHCs as soluble analytes for binding kinetics, because precise knowledge of the functional concentration is necessary to obtain correct curve fitting results.
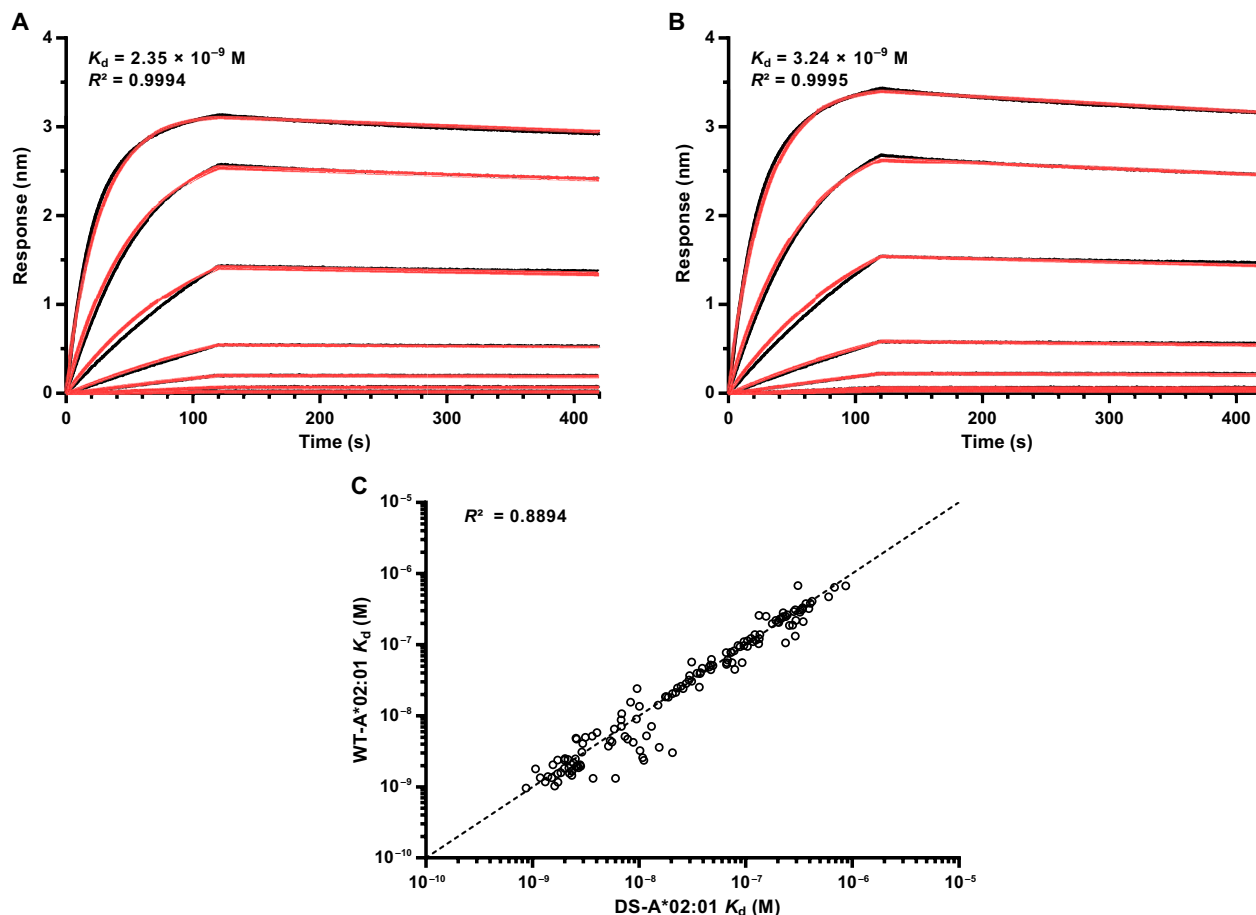
First, binding kinetics measurements were performed to measure binding of bs-868Z11-CD3 to the SL9 pMHC. Empty or SL9 peptide–loaded DS-A*02:01 molecules were immobilized on streptavidin biosensors and kinetics measured with soluble bs-868Z11-CD3. The binding affinities of bs-868Z11-CD3 for DS-A*02:01 SL9 and WT-A*02:01 SL9 pMHCs were similar at 2.35 and 3.24 nM, respectively (Fig. 4, A and B). Weak binding was measurable to functionally empty MHC molecules but not for irrelevantly loaded DS-A*02:01 complexes at a high molar concentration of 13.3 μM (fig. S1). Next, we analyzed bs-868Z11-CD3 binding affinities toward a positional scanning library based on the SL9 peptide sequence. This library was created by exchanging an amino acid at one position of the wild-type SL9 peptide against the 18 remaining proteinogenic amino acids while maintaining all other positions, resulting in 162 distinct peptides when performed at all positions of the nonamer (cysteine was excluded because of its propensity to dimerize) (25). pMHCs were generated either by addition of peptide to empty DS-A*02:01 molecules or by performing an ultraviolet (UV) light–mediated peptide ligand exchange, a technique also capable of pMHC generation after initial refolding (26). Respective pMHCs were immobilized on streptavidin biosensors, and kinetics were measured at two different bs-868Z11-CD3 concentrations. As expected, using alternate peptide

Fig. 4. Affinities of the SV9 specific bs-868Z11-CD3 bsTCR with different MHC monomers and peptide ligands. (**A**) Binding curve of bs-868Z11-CD3 against immobilized DS-A*02:01 SL9 pMHC. Raw data are displayed in black and curve fittings are in red. Measured using 1:2 analyte dilution series starting at 500 nM. (**B**) Binding curve of bs-868Z11-CD3 against immobilized WT-A*02:01 SL9 pMHC. Raw data are displayed in black and curve fittings are in red. Measured using 1:2 analyte dilution series starting at 500 nM. (**C**) Correlation between affinities measured using DS-A*02:01 pMHCs or WT-A*02:01 pMHCs generated using UV exchange. K_d values were plotted for 140 different peptide ligands generated using both methods and measured during successive experiments. K_d values were fitted using 500 and 158 nM analyte concentrations. Peptides were included if peak signal levels reached at least 0.05 nM for both concentrations and individual fits had a R^2 above 0.9. The in-picture R^2 is the calculated correlation coefficient, and dashed line represents optimal 1:1 ratio.

Because the functionally empty DS-A*02:01 molecule is stable without peptide, it offers less restrictions in this specific context: When added and kept in appropriate peptide concentration to saturate the MHCs, the effective concentration of pMHC can be expected to be equal to that of DS-A*02:01 initially supplied. Direct comparison of selected peptides from the positional scanning library prepared as soluble analytes, either through DS-A*02:01 peptide loading or UV exchange, did show decreased binding signals with UV exchange preparations for lower-affinity peptides, indicative of a reduced functional pMHC content (fig. S5A). This would have resulted in improper curve fittings and incorrect affinity constants (fig. S5B). Accurately measuring bsTCR affinities for such peptides can be important in the context of binding motif generation, because these substitutions may result in relevant MHC binders when combined with substitutions at other positions. Tolerance of these amino acids by the bsTCR should thus be reflected correctly in a comprehensive binding motif.

By immobilizing the bsTCR bs-868Z11-CD3 on a regenerable anti-F(ab) sensor, we were able to analyze the positional scanning library at four different soluble pMHC concentrations for each pep-tide ligand, ranging from 500 to 15.8 nM, within 4 hours of unattended measurement time and with 20-fold reduced cost compared with a matching pMHC immobilization setup. This measurement resulted in an informative pMHC-bsTCR binding motif (Fig. 5A and table S2). Soluble DS-A*02:01 pMHC preparations can be stored for at least 2 weeks at 4°C without loss of quality and used for multiple analyses (fig. S6).

The bsTCR bs-868Z11-CD3 displayed an expected pattern of recognition for a TCR: Changes of amino acids between positions 3 and 7 of SLYNTVATL, the region that directly interacts with the CDR3 loops of the scTv, had the biggest influence on bsTCR binding affinity. Replacements at these positions retaining strong binding were only possible with the few amino acids sharing the physiochemical characteristics of the parental amino acid. This behavior can also be graphically illustrated when visualizing the binding motif as Seq2Logo graph (Fig. 5B) (27). These results demonstrate that pMHCs can be generated quickly with the peptide-receptive DS-A*02:01 MHC molecule and are suitable as soluble analytes for high-throughput pMHC-bsTCR binding kinetics screenings.
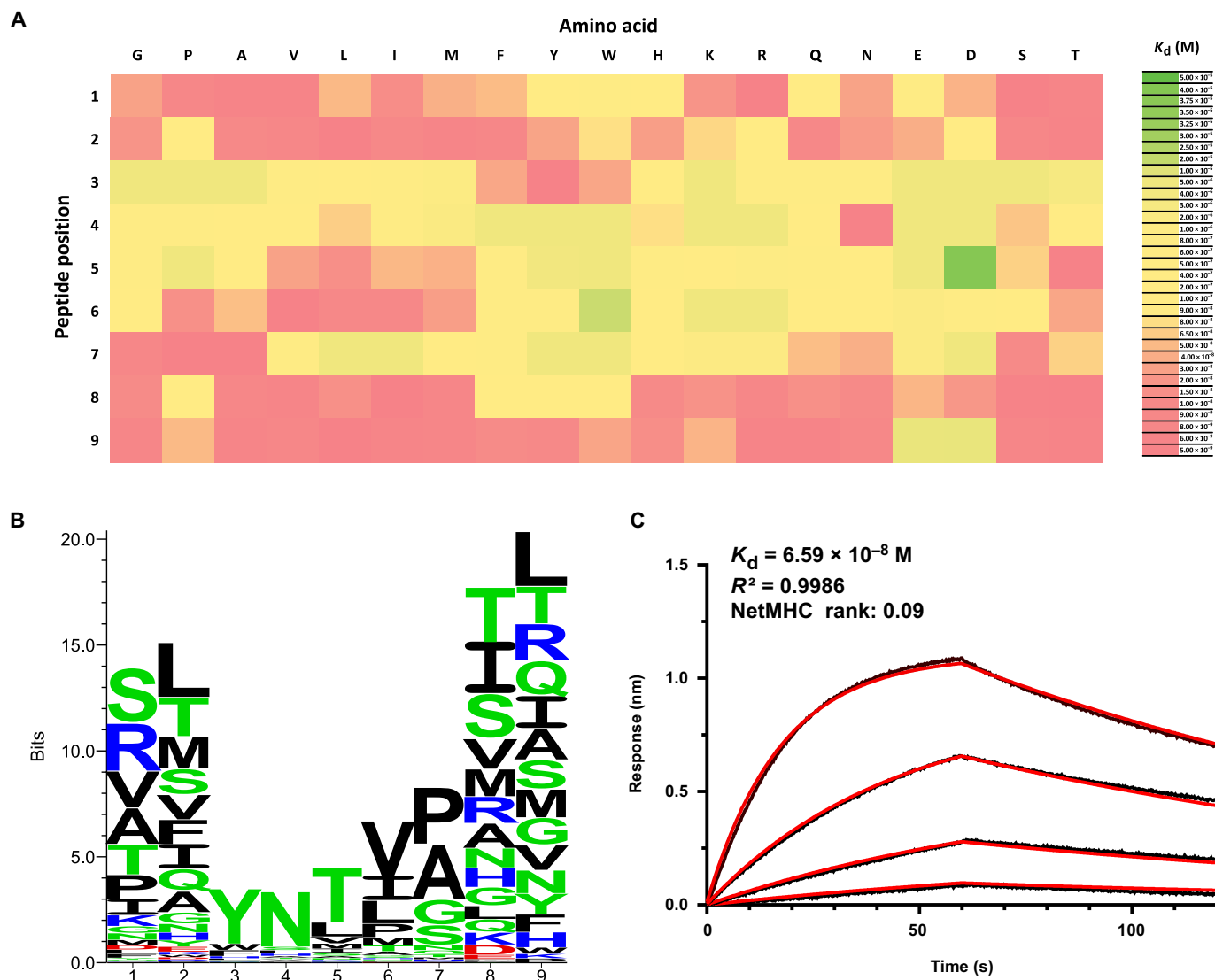
Fig. 5. Binding motif of bs-868Z11-CD3 generated using DS-A*02:01– generated positional scanning library as soluble analyte and immobilized bsTCR. Measurements were performed using four soluble analyte concentrations. Interactions without fittable curves were assigned a K_d value of 5 µM. Soluble analyte concentration range produced by 1:3.16 analyte dilution series starting at 500 nM. (**A**) Heatmap depicting bs-868Z11-CD3 affinities for the respective SLYNTVATL mutants from the positional scanning library. (**B**) Visualization of the binding motif as Seq2Logo graph. Size of individual letters inversely represents measured affinity for the respective amino acid at this position, calculated using the inverse K_d value divided by 10^8 and the PSSM-Logo algorithm. (**C**) Binding curve of bs-868Z11-CD3 bsTCR against ALYNVLAKV DS-A*02:01 pMHC. Measured using 1:3.16 analyte dilution series starting at 500 nM. Raw data are displayed in black and curve fittings are in red.

Identification of peptide ligands cross-reactive with bs-868Z11-CD3

We further wanted to demonstrate that we could use the generated binding motif to identify cross-reactive peptide ligands from the human proteome. We created a peptide ligand search motif from the binding affinity dataset using a K_d threshold of 50 nM: All single amino acid substitutions decreasing the bs-868Z11-CD3 affinity below that threshold were excluded from the motif (table S3).

On the basis of this motif, we performed a search in the National Center for Biotechnology Information (NCBI) human nonredundant protein sequence database for nonamer sequences matching combinations allowed by the motif. The search identified more than 400 hits within the proteome, with sequence identity to the wild-type sequence SLYNTVATL ranging from one to six identical posi-

tions. A total of 140 peptides were selected, sampled to be representative of the sequence identity distribution in the larger group, synthesized, and used for binding kinetics measurements (table S4). We were able to detect affinities of single-digit micromolar K_d values or larger for 91 of those peptides.

One of them, ALYNVLAKV, was worth of special notice because it is presented on the cell surface of multiple human tissue samples according to the XPRESIDENT immunopeptidomics database. This database combines quantitative HLA peptidomics based on liquid chromatography–mass spectrometry (LC-MS) analysis and quantitative transcriptomics provided by RNA sequencing from healthy tissues and tumor tissues to identify peptides presented exclusively or predominantly on tumor tissue (*28*, *29*). ALYNVLAKV, an antigen from intermediate filament family orphan 1 or 2 (IFFO1/2), was

detected on multiple healthy tissue and tumor tissue samples, ranging from the head and neck, spleen, or kidney to non–small cell lung carcinoma or renal cell carcinoma. The K_d value of the interaction was 65.9 nM (Fig. 5C). We were also able to identify a second LC-MS–detected peptide, KTFNLIPAV, with a lower affinity (K_d value of 413 nM), which was previously detected on three tumor tissue samples. Together, we show that pMHC-bsTCR binding motifs, generated with the high-throughput pMHC-bsTCR binding kinetics screening platform, can be used to identify cross-reactive peptide ligands, which occur in the human proteome and have the potential be presented as pMHCs.

Correlation of pMHC-bsTCR binding affinity with bsTCR-mediated T cell activation

Although pMHC-bsTCR binding affinity can be measured quickly using this high-throughput screening platform, it should correlate with the in vitro activity of the functional T cell–engaging bsTCR to be even more useful. Commonly, in vitro coincubations of target and effector cells coupled with an appropriate readout are used to characterize these constructs. T2 cells, a transporter associated with antigen processing (TAP)–deficient A*02:01 cell line with restorable pMHC presentation through exogenous peptide loading, were loaded separately with all peptides of the positional scanning library and the 140 selected peptides to serve as target cells. These were then incubated together with GloResponse NFAT-luc2 Jurkat effector cells, a cell line that expresses a luciferase reporter gene driven by a NFAT-response element, and different concentrations of bs-868Z11-CD3 (30, 31). Jurkat effector cell activation was detected after 18 hours by measuring bioluminescence.

We encountered a broad spectrum of activation levels against the positional scanning library, ranging from no detectable T cell activation with any bsTCR concentration to strong bioluminescence signals starting at low bsTCR concentrations, e.g., for the wild-type peptide (Fig. 6A). Because median effective concentration values could not be determined for every interaction with the selected bsTCR concentration range, we categorized the individual peptides by their bsTCR activation threshold, defined as the lowest bsTCR concentration that was able to induce a threefold increased bioluminescence signal compared with the background. These values were plotted for each peptide against the previously identified K_d values (Fig. 6B).

Overall, we detected a robust connection between the binding affinities and Jurkat effector cell activation. We also identified one group of outliers with strong pMHC-bsTCR binding affinities but higher activation thresholds than expected when compared with the overall trend. For the peptides of this group, the activation threshold seemed to increase in conjunction with decreasing peptide binding affinities for the MHC, based on predictions using the NetMHC 4.0 algorithm (Fig. 6C) (32).

This offered a potential explanation because different peptide binding affinities could result in different presentation levels of the respective pMHCs on the target cells after exogenous loading. These levels might, in turn, influence pMHC-bsTCR complex numbers and ultimately Jurkat effector cell activation. To corroborate the hypothesis, we performed a flow cytometric T2 peptide binding assay using an anti–HLA-A2 antibody and could detect less elevated HLA-A2 surface levels after peptide loading for peptides with lower binding affinities, especially NetMHC ranks of 2 and above, supporting the initial hypothesis (fig. S7).

Of the 140 peptide ligands selected by binding motif search, 24 could induce a threefold T cell activation over background with at least one of the supplied bsTCR concentrations (Fig. 6D). We found a similar connection between binding affinities and T cell activation compared with the results obtained with the positional scanning library. The previously highlighted IFFO1 peptide ALYNVLAKV was also reactive in the reporter assay (Fig. 6E).

In conclusion, we show that pMHC-bsTCR binding affinity is a good indicator for the in vitro function of the scTv 868Z11 coupled with an anti-CD3 T cell engager. This highlights the value of the pMHC-bsTCR binding kinetics screening platform because it allows quick but adequate characterization of bsTCRs early in the development of such molecules.

DISCUSSION

Here, we present a disulfide-stabilized and functionally empty HLA-A*02:01 molecule, which can be refolded and purified without the use of typically required high-affinity peptides. The resulting monomers can form pMHCs after addition of peptides in a one-step loading procedure. Although the disulfide bridge enhances the stability of the MHC molecule, introduction does not inhibit or substantially alter binding of TCRs to DS-A*02:01 pMHCs compared with the wild type.

This technique represents a great tool to quickly produce large pMHC libraries that are suitable for affinity measurements. Combining DS-A*02:01–produced pMHC libraries with biolayer interferometry–based analysis results in a platform capable of high-throughput pMHC-bsTCR binding kinetics screenings. This setup could also be useful for the analysis of other biologics targeting pMHCs, like monoclonal antibodies or bispecifics, such as bispecific T cell engagers.

In one application of this platform, we were able to quickly collect a pMHC-bsTCR binding affinity dataset for the HIV-specific bsTCR bs-868Z11-CD3. bsTCR binding affinities for respective pMHCs were indicative of in vitro activity when coupled with the presented T cell engager and tested in a cellular reporter assay, making these datasets valuable for bsTCR characterization. Analysis of the relationship between binding affinity and bsTCR-mediated cellular activation over a wide range of pMHC-bsTCR affinities has been difficult, thus far as a result of the limited tools available to feasibly collect such datasets.

The collected binding motif revealed similarities to the binding motif of the wild-type TCR 868. Analysis of an 868-SV9 crystal structure, as well as an accompanying alanine scan by Cole et al. (33), revealed prominent interactions between the CDR3α region and the amino acids 4N and 5T of SLYNTVATL. This behavior seems to be conserved although a significant part of the CDR3α is mutated in the 868Z11 construct. Using the binding motif and a model search strategy, we were able to identify multiple peptides from the human proteome, which demonstrated high-affinity interactions with the bsTCR and the potential to induce bsTCR-mediated Jurkat effector activation when presented on target cells.

Note that TCR binding motifs derived from single amino acid substitution libraries may still not reflect all possible peptides a specific TCR can recognize, because the exchange of multiple amino acids, at the same time, might have different effects than the isolated exchanges. Alternative approaches include screening of more complex libraries, for example, through target cell loading with high diversity peptide pools, each randomized at all but one position of
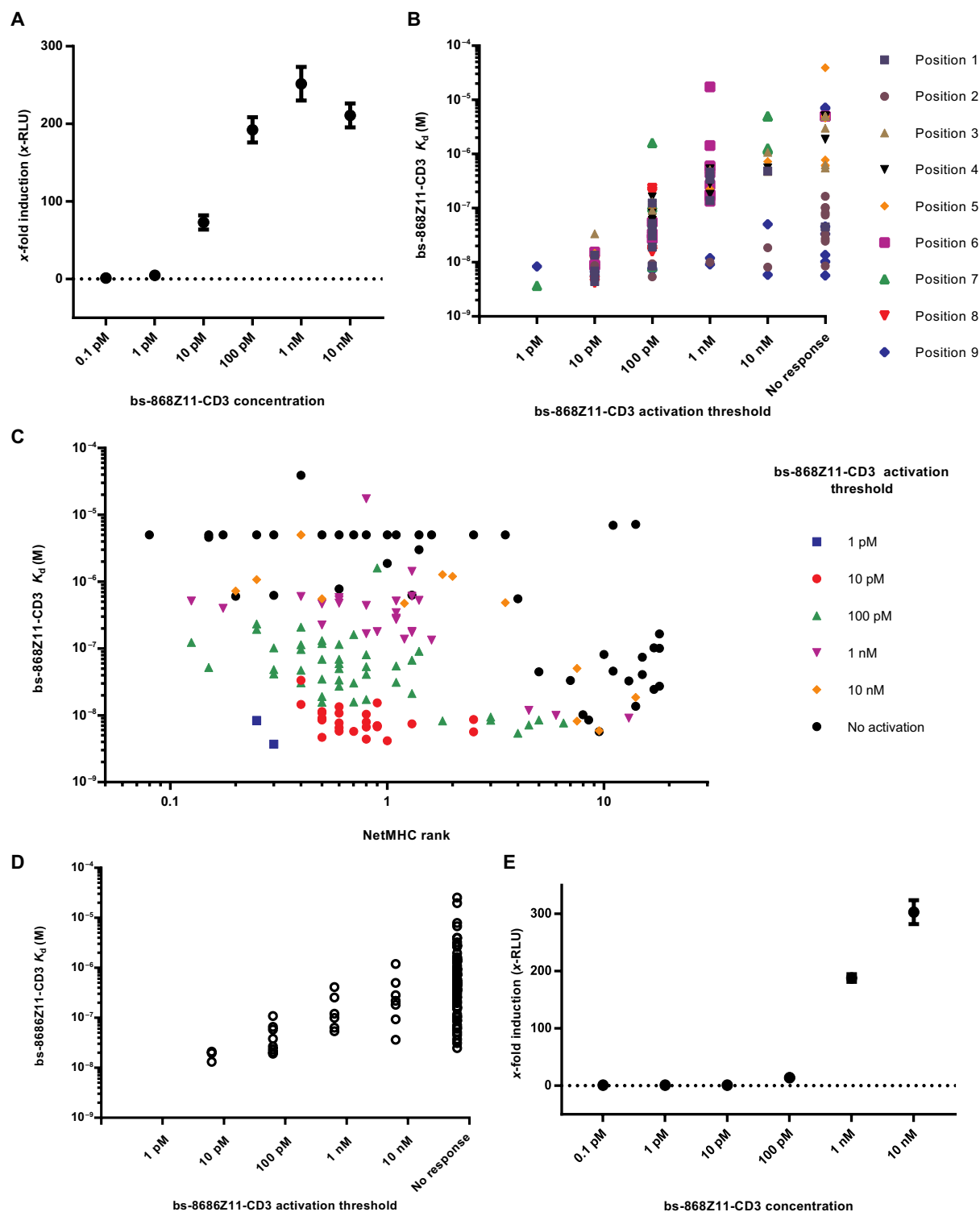
Fig. 6. Result of coincubation assays with peptide-loaded target cells, Jurkat effector cells, and bs-868Z11-CD3 at six different concentrations. (**A**) Measured fold induction above background for Jurkat effector cells activated at different concentrations of bs-868Z11-CD3 against SL9 peptide–loaded T2 target cells. Error bars represent biological triplicates. (**B**) Measured binding affinities for peptide ligands from the positional scanning library and their respective bsTCR activation threshold and the lowest bsTCR concentration necessary to induce Jurkat effector cell activation threefold over background based on bioluminescence. Peptides are grouped on the basis of the location of the exchange in the wild-type sequence. (**C**) Measured binding affinities for peptide ligands from the positional scanning library and their respective NetMHC-predicted binding rank. Peptides are grouped on the basis of the bsTCR activation threshold. (**D**) Measured binding affinities for the cross-reactive peptide ligand candidates and their respective bsTCR activation threshold. (**E**) Measured fold induction above background for Jurkat effector cells stimulated at different concentrations of bs-868Z11-CD3 against ALYNVLAKV peptide–loaded T2 target cells. Error bars represent biological triplicates.

the peptide, or screenings against randomized peptide libraries presented as pMHC molecules on yeast surfaces (*10*, *34*, *35*). Further research directly comparing these approaches will be necessary to gain a deeper understanding of the respective strengths and weaknesses. Ultimately, safety screenings of clinical candidates should always be composed of multiple approaches, for example, by combining binding motif guided analysis together with cellular screenings of large panels of healthy tissue–derived cell lines, to minimize risks.

Nevertheless, our results highlight the capability of this approach to identifying potentially relevant off-target interactions in combination with the pMHC-bsTCR binding kinetics screening platform. Because it offers quick analysis of complex pMHC libraries, it can be used early in the development process to select promising candidates and thus complements established methods.

This platform can also facilitate larger and more comprehensive screenings of late-stage candidates, potentially against mass spectrometry data-driven tissue-specific pMHC libraries covering the known immunopeptidome. Because of its stability and low-effort peptide loading procedure, the DS-A*02:01 molecule could potentially enable even higher-throughput platforms. Thanks to these properties, it could be perfectly suited for the creation of high complexity pMHC microarrays with thousands of different pMHCs, for example, by combining large-scale coating of DS-A*02:01 and modern high-throughput peptide microarray inkjet printers.

MATERIALS AND METHODS
Study design
The goal of this study was to test and characterize a newly developed disulfide-stabilized empty HLA-A*02:01 molecule as a tool to generate large libraries of high-quality pMHCs and to demonstrate its use as a high-throughput kinetic screening platform for the screening of bispecific T cell engagers.

Peptide synthesis
All peptides were generated in-house using standard 9-fluorenyl methoxycarbonyl chemistry with a Syro II peptide synthesizer. Peptides were subsequently analyzed using high-performance liquid chromatography (HPLC) and had an average purity of 74%. UV light–sensitive peptides contained a light-sensitive building block with a 2-nitrophenylamino acid residue. The dipeptide GM was procured from Bachem. Before use, peptides were dissolved in dimethyl sulfoxide (DMSO; catalog no. 41640, Sigma-Aldrich) and 0.5% trifluoroacetic acid (TFA; catalog no. T6508, Sigma-Aldrich) at concentrations ranging from 2 to 10 mg ml^{-1} depending on the desired use case.

Generation of MHCs by refolding and purification
Recombinant HLA-A*02:01 wild type (WT-A*02:01) or the HLA-A*02:01 disulfide mutant (DS-A*02:01) heavy chain with C-terminal BirA signal sequences and human β_2m light chain was produced in *E. coli* as inclusion bodies and purified as previously described (*2*). HLA-A*02:01 complex refolding reactions were performed as previously described with minor modifications (*18*). Briefly, WT-A*02:01 or DS-A*02:01 heavy chain, β_2m light chain, and peptide were diluted in refolding buffer [100 mM tris-Cl (pH 8), 0.5 M arginine, 2 mM EDTA, 0.5 mM oxidized glutathione, and 5 mM reduced glutathione] and incubated for 2 to 8 days at 4°C while stirring before concentration. The concentrated protein was purified by SEC in 20 mM tris-HCl (pH 8)/150 mM

NaCl on an ÄKTAprime system (GE Healthcare) using a HiLoad 26/600 Superdex 200 pg column (GE Healthcare). Peak fraction was either concentrated directly to 2000 µg ml^{-1}, aliquoted and frozen at −80°C or biotinylated by BirA biotin protein ligase (Avidity) overnight at 4°C according to the manufacturer's instructions, and subjected to a second gel filtration before final concentration to 2000 µg ml^{-1}, aliquoting and storage at −80°C. To produce WT-A*02:01 pMHCs, full-length peptides or UV light–sensitive full-length peptides were added to the refolding buffer at a concentration of 30 µM. To produce DS-A*02:01 complexes, the dipeptide GM was added to the refolding buffer at a concentration of 10 mM.

Generation of peptide-exchanged HLA-A*02:01 pMHCs using UV-mediated peptide ligand exchange or empty DS-A*02:01 complexes
Peptide exchange reactions with UV light–cleavable peptides were performed as previously described (*26*). In short, desired nonamer peptides were mixed with biotinylated UV light–sensitive pMHCs at 100:1 molar ratio and subjected to at least 30 min of 366-nm UV light (CAMAG). Peptide loading reactions with empty DS-A*02:01 MHCs were performed by addition and mixing of desired peptides with at least a 100:1 molar ratio to the monomer solution and 5-min incubation at room temperature.

Soluble TCR production
Soluble TCRs were produced as previously described (*21*). In short, TCRα and TCRβ chain constructs were expressed separately in *E. coli* as inclusion bodies and purified. TCRα chains were mutated at position 48 by replacing a threonine with a cysteine and TCRβ chains at position 57 by replacing a serine with a cysteine to form an interchain disulfide bond.

bsTCR design and production
The bs-868Z11-CD3 molecule was generated by linking the scTv 868Z11 to the C terminus of the F(ab′) domain of a humanized anti-CD3 antibody (*23*, *24*). To this end, the V$_\beta$ domain of the scTv was directly fused to the upper CH2 region derived from human immunoglobulin G2 (APPVAG). Cysteine knockouts C226S and C229S within the hinge prevent the formation of F(ab′)$_2$ molecules. Human cytomegalovirus–driven expression vectors coding either for the construct described above or for the light chain of the humanized anti-CD3 antibody were transiently cotransfected in ExpiCHO cells (Thermo Fisher Scientific). After 12 days, the supernatant was processed by tandem chromatography (protein L followed by preparative size exclusion; GE Healthcare), and highly pure monomeric bsTCR was formulated in phosphate-buffered saline (PBS).

Crystallization and imaging
The DS-A*02:01 ESO 9V complex and the 1G4 TCR were concentrated and mixed in a 1:1 ratio to achieve a concentration of 7 mg ml^{-1} for crystallization. A sitting drop vapor diffusion experiment resulted in crystals in the presence of a mother liquor containing 0.1 M ammonium acetate, 0.1 M bis-tris (pH 5.5), and 17% polyethylene glycol (PEG) 10,000. A single crystal was transferred to a cryoprotectant solution containing 0.1 M ammonium acetate, 0.1 M bis-tris (pH 5.5), 20% (w/v) PEG 10,000, and 10% glycerol. The crystal was mounted and cryocooled at 100 K on the EMBL P14 beamline at Deutsche Elektronen-Synchrotron containing an EIGER 16M detector. An x-ray dataset was collected to a resolution of 2.5 Å (table S1).

The data were processed with X-ray Detector Software (XDS) and scaled with AIMLESS (*36*, *37*). Molecular replacement was performed using MOLREP with the coordinates of the TCR portion of the native complex first, followed by the pMHC [Protein Data Bank (PDB) 2BNR], and the structure was refined with REFMAC5 (*38*, *39*). The engineered disulfide bond was manually built with Coot (*40*). The structure was refined to an *R* factor of 22.9% (R_{free} of 27.3%). MolProbity was used to validate the geometry and indicated that 93.9% of the residues were in the allowed regions of the Ramachandran plot [with one glycine residue (Gly^{143}) in the disallowed regions] (*41*).

Octet RED384–based biolayer interferometry binding kinetics measurements
The affinity of sTCR or bsTCR molecules for different pMHCs was measured on an Octet RED384 system (Pall FortéBio) using kinetic or steady-state binding analysis. All analytes or ligands were diluted to their final concentration in kinetics buffer [PBS, 0.1% bovine serum albumin, and 0.05% Tween 20], if not specified otherwise. All biosensors were hydrated for at least 10 min in kinetics buffer before use. Loadings and measurements were performed in 384 tilted well plates (Pall FortéBio) with at least 40 µl at a 3-mm sensor offset. Plate temperature was set at 25°C and shaker speed at 1000 rpm. To allow interstep correction, baselines before association phases and the following dissociation phase were performed in the same well. Kinetics buffer was used as dissociation buffer with DMSO at an appropriate concentration added, if necessary to match the analyte composition. In the case of pMHC immobilization, dip and read streptavidin (catalog no. 18-5021, Pall FortéBio) biosensors were used to immobilize biotinylated pMHC monomers at a presumed concentration of 25 µg ml^{-1} for 60 s, followed by a 60-s baseline and association and dissociation phases of 60 s each, if not specified otherwise. In the case of bsTCR immobilization, dip and read anti-human Fab-CH1 second generation (FAB2G; catalog no. 18-5127, Pall FortéBio) biosensors were used to immobilize bsTCR molecules at a concentration of 100 µg ml^{-1} for 60 s, followed by a 15-s baseline and association and dissociation phases of 60 s each, if not specified otherwise. FAB2G biosensors were regenerated up to four times by incubating the loaded biosensor for 5 s each in 10 mM glycine (pH 1.5) and kinetics buffer consecutively for three times. FAB2G were also preconditioned that way before their first ligand immobilization.

All sensorgrams were analyzed using the Octet RED384 system software "Data Analysis HT" version 10.0.3.7 (Pall FortéBio). Raw sensor data were aligned at the *y* axis by aligning the data to the end of the baseline step, and interstep correction was used to align the start of the dissociation to the end of the association phase. No Savitzky-Golay filtering was applied. Resulting sensorgrams were then fitted using a 1:1 Langmuir kinetics binding model.

Cell lines
The TAP-deficient HLA-A*02:01–expressing cell line T2 was procured from American Type Culture Collection (CRL-1992) and cultured in RPMI 1640 GlutaMAX (catalog no. 61870010, Thermo Fisher Scientific) supplemented with 10% heat-inactivated fetal bovine serum (FBS; catalog no. 10270106, Life Technologies) and the antibiotics penicillin and streptomycin (100 µg ml^{-1} each; catalog no. 882082, Biozym) up until passage number 16, if necessary. The GloResponse NFAT-luc2 Jurkat cell line was procured from Promega (catalog no. CS1764) at passage number 6 and cultured in RPMI 1640 GlutaMAX (catalog no. 61870010, Thermo Fisher Scientific) supplemented with 10%

heat-inactivated FBS (catalog no. 10270106, Life Technologies), 1% sodium pyruvate (catalog no. Z-20M, c.c.pro), the antibiotics hygromycin B (200 µg ml^{-1}; catalog no. 400052, Merck Millipore), and penicillin and streptomycin (100 µg ml^{-1} each; catalog no. 882082, Biozym) up until passage number 14, if necessary.

T cell activation assay
T cell activation assays using GloResponse NFAT-luc2 Jurkat cells and peptide-loaded T2 target cells were performed according to manufacturers' instructions. In short, T2 cells were harvested from continuous cell culture, washed and resuspended in T2 culture medium at a concentration of 3.3×10^6 cells ml^{-1}, and transferred to 96-well round-bottom plates (catalog no. 3799, Corning Costar). Peptide in DMSO and 0.5% TFA was added to a final concentration of 100 nM, and the suspension was incubated for 2 to 3 hours at 37°C in 5% CO_2. bsTCR formulated in PBS was diluted in T2 culture medium to desired concentration, and 25 µl of the respective dilution was distributed to white 96-well flat-bottom plates (catalog no. 781965, BRAND). GloResponse NFAT-luc2 Jurkat cells were harvested from continuous cell culture and washed and resuspended in T2 culture medium at a concentration of 3.0×10^6 cells ml^{-1}, and 25 µl of the cell suspension was distributed to the white 96-well flat-bottom plates with bsTCR dilutions.

After peptide loading, T2 cells were resuspended, and 25 µl of the cell suspension was distributed to the white 96-well flat-bottom plates with bsTCR dilutions and GloResponse NFAT-luc2 Jurkat cells for a final effector-to-target ratio of 1:1 (75,000 cells each). Fully assembled plates were mixed for 5 min at 300 rpm on a plate shaker and then incubated for 18 to 20 hours at 37°C in 5% CO_2. After the incubation period, 75 µl of Bio-Glo luciferase reagent was added to each well, and the plates incubated for minutes at 300 rpm on a plate shaker in the dark before reading luminescence at a 0.5-s integration time with a Synergy2 plate reader (BioTek). Luminescence as measured in relative light units (RLUs) was converted to fold induction for each well by dividing measured RLUs by that of control wells.

Motif-based identification of potentially cross-reactive peptide ligands
Searches for nonamer peptide ligands matching one of the potential combinations allowed by the search motif were performed using the NCBI human protein database. This database covers all nonredundant GenBank CDS translations, as well as records from PDB, SwissProt, Protein Information Resource (PIR), and Protein Research Foundation (PRF) but excluding environmental samples from the whole-genome shotgun projects. The database was directly acquired from the NCBI servers.

Seq2Logo generation
Seq2Logos visualizing the binding motif were created by taking the inverse value of measured K_d values for the respective interaction and dividing them by 10^8. These values were assembled in the form of a position-specific scoring matrix file and processed using the Position-Specific Scoring Matrix (PSSM)–Logo type at the Seq2Logo online resource of the Denmark Technical University Bioinformatics department (*27*).

Statistical analysis
All data were plotted using the GraphPad Prism software version 7. Correlation between *x* and *y* datasets were calculated by computing

the Pearson correlation coefficient and were reported as R^2 using the GraphPad Prism software version 7. R^2 and X^2 values for curve fittings of biolayer interferometry binding kinetics measurements were calculated using the Octet RED384 system software Data Analysis HT version 10.0.3.7.

SUPPLEMENTARY MATERIALS

immunology.sciencemag.org/cgi/content/full/4/37/eaav0860/DC1
Methods
Fig. S1. Binding of multiple different soluble TCRs and bsTCR bs-868Z11-CD3 to nonloaded DS-A*02:01 or DS-A*02:01 loaded with an irrelevant peptide.
Fig. S2. Analysis of DS-A*02:01 peptide receptiveness after different storage durations at −80°C measured by fluorescence anisotropy.
Fig. S3. Illustration of bsTCR bs-868Z11-CD3 construct.
Fig. S4. R_{max} values reported for immobilized DS-A*02:01 and UV exchange generated WT-A*02:01 pMHCs.
Fig. S5. Analysis of UV exchange efficiency and Octet measurement results for 28 different peptides selected from SLYNTVATL-based positional scanning library.
Fig. S6. Octet binding kinetics measurements for DS-A*02:01 SLYNTVATL pMHC with immobilized bs-868Z11-CD3 directly after exchange and after 2 weeks of storage at 4°C.
Fig. S7. Flow cytometric peptide binding assay with an anti-human HLA-A2 antibody staining of T2 cells after exogenous peptide loading.
Table S1. Data collection and refinement statistics 1G4/DS-A*02:01/ESO 9V.
Table S2. bs-868Z11-CD3 binding affinity against SV9 peptide SLYNTVATL and peptides from positional scanning library.
Table S3. Cross-reactive peptide ligand search motif for bs-868Z11-CD3 based on the binding affinities measured using the positional scanning library.
Table S4. bs-868Z11-CD3 binding affinity for selected peptide ligands identified on the basis of the bs-868Z11-CD3 binding motif.
Table S5. Raw data (Excel file).

REFERENCES AND NOTES

1. H. G. Rammensee, K. Falk, O. Rötzschke, Peptides naturally presented by MHC class I molecules. *Annu. Rev. Immunol.* **11**, 213–244 (1993).
2. D. N. Garboczi, D. T. Hung, D. C. Wiley, HLA-A2-peptide complexes: Refolding and crystallization of molecules expressed in Escherichia coli and complexed with single antigenic peptides. *Proc. Natl. Acad. Sci. U.S.A.* **89**, 3429–3433 (1992).
3. J. D. Altman, P. A. H. Moss, P. J. R. Goulder, D. H. Barouch, M. G. McHeyzer-Williams, J. I. Bell, A. J. McMichael, M. M. Davis, Phenotypic analysis of antigen-specific T lymphocytes. *Science* **274**, 94–96 (1996).
4. S. R. Hadrup, M. Toebes, B. Rodenko, A. H. Bakker, D. A. Egan, H. Ovaa, T. N. M. Schumacher, High-throughput T-cell epitope discovery through MHC peptide exchange. *Methods Mol. Biol.* **524**, 383–405 (2009).
5. K. C. Garcia, M. D. Tallquist, L. R. Pease, A. Brunmark, C. A. Scott, M. Degano, E. A. Stura, P. A. Peterson, I. A. Wilson, L. Teyton, Alphabeta T cell receptor interactions with syngeneic and allogeneic ligands: Affinity measurements and crystallization. *Proc. Natl. Acad. Sci. U.S.A.* **94**, 13838–13843 (1997).
6. J. D. Stone, D. M. Kranz, Role of T cell receptor affinity in the efficacy and specificity of adoptive T cell therapies. *Front. Immunol.* **4**, 1–16 (2013).
7. P. F. Robbins, Y. F. Li, M. El-Gamil, Y. Zhao, J. A. Wargo, Z. Zheng, H. Xu, R. A. Morgan, S. A. Feldman, L. A. Johnson, A. D. Bennett, S. M. Dunn, T. M. Mahon, B. K. Jakobsen, S. A. Rosenberg, Single and dual amino acid substitutions in TCR CDRs can enhance antigen-specific T cell functions. *J. Immunol.* **180**, 6116–6131 (2008).
8. A. Varela-Rohena, P. E. Molloy, S. M. Dunn, Y. Li, M. M. Suhoski, R. G. Carroll, A. Milicic, T. Mahon, D. H. Sutton, B. Laugel, R. Moysey, B. J. Cameron, A. Vuidepot, M. A. Purbhoo, D. K. Cole, R. E. Phillips, C. H. June, B. K. Jakobsen, A. K. Sewell, J. L. Riley, Control of HIV-1 immune escape by CD8 T cells expressing enhanced T-cell receptor. *Nat. Med.* **14**, 1390–1395 (2008).
9. J. Oates, N. J. Hassan, B. K. Jakobsen, ImmTACs for targeted cancer therapy: Why, what, how, and which. *Mol. Immunol.* **67**, 67–74 (2015).
10. L. Wooldridge, J. Ekeruche-Makinde, H. A. van den Berg, A. Skowera, J. J. Miles, M. P. Tan, G. Dolton, M. Clement, S. Llewellyn-Lacey, D. A. Price, M. Peakman, A. K. Sewell, A single autoimmune T cell receptor recognizes more than a million different peptides. *J. Biol. Chem.* **287**, 1168–1177 (2012).
11. B. J. Cameron, A. B. Gerry, J. Dukes, J. V. Harper, V. Kannan, F. C. Bianchi, F. Grand, J. E. Brewer, M. Gupta, G. Plesa, G. Bossi, A. Vuidepot, A. S. Powlesland, A. Legg, K. J. Adams, A. D. Bennett, N. J. Pumphrey, D. D. Williams, G. Binder-Scholl, I. Kulikovskaya, B. L. Levine, J. L. Riley, A. Varela-Rohena, E. A. Stadtmauer, A. P. Rapoport, G. P. Linette, C. H. June, N. J. Hassan, M. Kalos, B. K. Jakobsen, Identification of a Titin-derived HLA-A1-presented peptide as a cross-reactive target for engineered MAGE A3-directed T cells. *Sci. Transl. Med.* **5**, 197ra103 (2013).
12. G. P. Linette, E. A. Stadtmauer, M. V. Maus, A. P. Rapoport, B. L. Levine, L. Emery, L. Litzky, A. Bagg, B. M. Carreno, P. J. Cimino, G. K. Binder-Scholl, D. P. Smethurst, A. B. Gerry, N. J. Pumphrey, A. D. Bennett, J. E. Brewer, J. Dukes, J. Harper, H. K. Tayton-Martin, B. K. Jakobsen, N. J. Hassan, M. Kalos, C. H. June, Cardiovascular toxicity and titin cross-reactivity of affinity-enhanced T cells in myeloma and melanoma. *Blood* **122**, 863–871 (2013).
13. M. C. C. Raman, P. J. Rizkallah, R. Simmons, Z. Donnellan, J. Dukes, G. Bossi, G. S. Le Provost, P. Todorov, E. Baston, E. Hickman, T. Mahon, N. Hassan, A. Vuidepot, M. Sami, D. K. Cole, B. K. Jakobsen, Direct molecular mimicry enables off-target cardiovascular toxicity by an enhanced affinity TCR designed for cancer immunotherapy. *Sci. Rep.* **6**, 18851 (2016).
14. H. M. Bijen, D. M. van der Steen, R. S. Hagedoorn, A. K. Wouters, L. Wooldridge, J. H. F. Falkenburg, M. H. M. Heemskerk, Preclinical strategies to identify off-target toxicity of high-affinity TCRs. *Mol. Ther.* **26**, 1206–1214 (2018).
15. W. Shao, P. G. A. Pedrioli, W. Wolski, C. Scurtescu, E. Schmid, J. A. Vizcaíno, M. Courcelles, H. Schuster, D. Kowalewski, F. Marino, C. S. L. Arlehamn, K. Vaughan, B. Peters, A. Sette, T. H. M. Ottenhoff, K. E. Meijgaarden, N. Nieuwenhuizen, S. H. E. Kaufmann, R. Schlapbach, J. C. Castle, A. I. Nesvizhskii, M. Nielsen, E. W. Deutsch, D. S. Campbell, R. L. Moritz, R. A. Zubarev, A. J. Ytterberg, A. W. Purcell, A. Marcilla, A. Paradela, Q. Wang, C. E. Costello, N. Ternette, P. A. van Veelen, C. A. C. M. van Els, A. J. R. Heck, G. A. de Souza, L. M. Sollid, A. Admon, S. Stevanovic, H. G. Rammensee, P. Thibault, C. Perreault, M. Bassani-Sternberg, R. Aebersold, E. Caron, The SysteMHC Atlas project. *Nucleic Acids Res.* **46**, D1237–D1247 (2018).
16. M. Zacharias, S. Springer, Conformational flexibility of the MHC class I α1-α2 domain in peptide bound and free states: A molecular dynamics simulation study. *Biophys. J.* **87**, 2203–2214 (2004).
17. Z. Hein, H. Uchtenhagen, E. T. Abualrous, S. K. Saini, L. Janssen, A. van Hateren, C. Wiek, H. Hanenberg, F. Momburg, A. Achour, T. Elliott, S. Springer, D. Boulanger, Peptide-independent stabilization of MHC class I molecules breaches cellular quality control. *J. Cell Sci.* **127**, 2885–2897 (2014).
18. S. K. Saini, E. T. Abualrous, A. S. Tigan, K. Covella, U. Wellbrock, S. Springer, Not all empty MHC class I molecules are molten globules: Tryptophan fluorescence reveals a two-step mechanism of thermal denaturation. *Mol. Immunol.* **54**, 386–396 (2013).
19. S. K. Saini, K. Ostermeir, V. R. Ramnarayan, H. Schuster, M. Zacharias, S. Springer, Dipeptides promote folding and peptide binding of MHC class I molecules. *Proc. Natl. Acad. Sci. U.S.A.* **110**, 15383–15388 (2013).
20. S. K. Saini, T. Tamhane, R. Anjanappa, A. Saikia, S. Ramskov, M. Donia, I. M. Svane, S. N. Jakobsen, M. Garcia-Alai, M. Zacharias, R. Meijers, S. Springer, S. R. Hadrup, Empty peptide-receptive MHC class I molecules for efficient detection of antigen-specific T cells. *Sci. Immunol.* **7**, eaau9039 (2019).
21. J. M. Boulter, M. Glick, P. T. Todorov, E. Baston, M. Sami, P. Rizkallah, B. K. Jakobsen, Stable, soluble T-cell receptor molecules for crystallization and therapeutics. *Protein Eng.* **16**, 707–711 (2003).
22. J.-L. Chen, G. Stewart-Jones, G. Bossi, N. M. Lissin, L. Wooldridge, E. M. L. Choi, G. Held, P. R. Dunbar, R. M. Esnouf, M. Sami, J. M. Boulter, P. Rizkallah, C. Renner, A. Sewell, P. A. van der Merwe, B. K. Jakobsen, G. Griffiths, E. Y. Jones, V. Cerundolo, Structural and kinetic basis for heightened immunogenicity of T cell vaccines. *J. Exp. Med.* **201**, 1243–1255 (2005).
23. D. H. Aggen, A. S. Chervin, F. K. Insaidoo, K. H. Piepenbrink, B. M. Baker, D. M. Kranz, Identification and engineering of human variable regions that allow expression of stable single-chain T cell receptors. *Protein Eng. Des. Sel.* **24**, 361–372 (2011).
24. Z. Zhu, P. Carter, Identification of heavy chain residues in a humanized anti-CD3 antibody important for efficient antigen binding and T cell activation. *J. Immunol.* **155**, 1903–1910 (1995).
25. S. R. Burrows, S. J. Rodda, A. Suhrbier, H. M. Geysen, D. J. Moss, The specificity of recognition of a cytotoxic T lymphocyte epitope. *Eur. J. Immunol.* **22**, 191–195 (1992).
26. B. Rodenko, M. Toebes, S. R. Hadrup, W. J. E. van Esch, A. M. Molenaar, T. N. M. Schumacher, H. Ovaa, Generation of peptide-MHC class I complexes through UV-mediated ligand exchange. *Nat. Protoc.* **1**, 1120–1132 (2006).
27. M. C. F. Thomsen, M. Nielsen, Seq2Logo: A method for construction and visualization of amino acid binding motifs and sequence profiles including sequence weighting, pseudo counts and two-sided representation of amino acid enrichment and depletion. *Nucleic Acids Res.* **40**, W281–W287 (2012).
28. T. Weinschenk, C. Gouttefangeas, M. Schirle, F. Obermayr, S. Walter, O. Schoor, R. Kurek, W. Loeser, K. H. Bichler, D. Wernet, S. Stevanović, H. G. Rammensee, Integrated functional genomics approach for the design of patient-individual antitumor vaccines. *Cancer Res.* **62**, 5818–5827 (2002).
29. J. Fritsche, B. Rakitsch, F. Hoffgaard, M. Römer, H. Schuster, D. J. Kowalewski, M. Priemer, V. Stos-Zweifel, H. Hörzer, A. Satelli, A. Sonntag, V. Goldfinger, C. Song, A. Mahr, M. Ott, O. Schoor, T. Weinschenk, Translating immunopeptidomics to immunotherapy-decision-making for patient and personalized target selection. *Proteomics* **18**, e1700284 (2018).

30. T. Elliott, A. Willis, V. Cerundolo, A. Townsend, Processing of major histocompatibility class I-restricted antigens in the endoplasmic reticulum. *J. Exp. Med.* **181**, 1481–1491 (1995).

31. G. Bossi, A. B. Gerry, S. J. Paston, D. H. Sutton, N. J. Hassan, B. K. Jakobsen, Examining the presentation of tumor-associated antigens on peptide-pulsed T2 cells. *Oncoimmunology* **2**, e26840 (2014).

32. M. Andreatta, M. Nielsen, Gapped sequence alignment using artificial neural networks: Application to the MHC class I system. *Bioinformatics* **32**, 511–517 (2016).

33. D. K. Cole, A. Fuller, G. Dolton, E. Zervoudi, M. Legut, K. Miles, L. Blanchfield, F. Madura, C. J. Holland, A. M. Bulek, J. S. Bridgeman, J. J. Miles, A. J. A. Schauenburg, K. Beck, B. D. Evavold, P. J. Rizkallah, A. K. Sewell, Dual molecular mechanisms govern escape at immunodominant HLA A2-restricted HIV epitope. *Front. Immunol.* **8**, 1503 (2017).

34. M. E. Birnbaum, J. L. Mendoza, D. K. Sethi, S. Dong, J. Glanville, J. Dobbins, E. Özkan, M. M. Davis, K. W. Wucherpfennig, K. C. Garcia, Deconstructing the peptide-MHC specificity of t cell recognition. *Cell* **157**, 1073–1087 (2014).

35. M. H. Gee, A. Han, S. M. Lofgren, J. F. Beausang, J. L. Mendoza, M. E. Birnbaum, M. T. Bethune, S. Fischer, X. Yang, R. Gomez-Eerland, D. B. Bingham, L. V. Sibener, R. A. Fernandes, A. Velasco, D. Baltimore, T. N. Schumacher, P. Khatri, S. R. Quake, M. M. Davis, K. C. Garcia, Antigen identification for orphan T cell receptors expressed on tumor-infiltrating lymphocytes. *Cell* **172**, 549–563.16 (2018).

36. W. Kabsch, XDS. *Acta Crystallogr. D Biol. Crystallogr.* **66**, 125–132 (2010).

37. P. Evans, Scaling and assessment of data quality. *Acta Crystallogr. Sect. D Biol. Crystallogr.* **62**, 72–82 (2006).

38. A. Vagin, A. Teplyakov, Molecular replacement with MOLREP. *Acta Crystallogr. Sect. D Biol. Crystallogr.* **66**, 22–25 (2010).

39. O. Kovalevskiy, R. A. Nicholls, F. Long, A. Carlon, G. N. Murshudov, Overview of refinement procedures within REFMAC 5: Utilizing data from different sources. *Acta Crystallogr. Sect. D Struct. Biol.* **74**, 215–227 (2018).

40. P. Emsley, B. Lohkamp, W. G. Scott, K. Cotwan, Features and development of Coot. *Acta Crystallogr. Sect. D Biol. Crystallogr.* **66**, 486–501 (2010).

41. V. B. Chen, W. B. Arendall III, J. J. Headd, D. A. Keedy, R. M. Immormino, G. J. Kapral, L. W. Murray, J. S. Richardson, D. C. Richardson, MolProbity: All-atom structure validation for macromolecular crystallography. *Acta Crystallogr. Sect. D Biol. Crystallogr.* **66**, 12–21 (2010).

Science Immunology

High-throughput peptide-MHC complex generation and kinetic screenings of TCRs with peptide-receptive HLA-A*02:01 molecules

Andreas Moritz, Raghavendra Anjanappa, Claudia Wagner, Sebastian Bunk, Martin Hofmann, Gabriele Pszolla, Ankur Saikia, Maria Garcia-Alai, Rob Meijers, Hans-Georg Rammensee, Sebastian Springer, and Dominik Maurer

Empty MHC reagents improve T cell detection

Recombinant MHC molecules displaying single peptides in their peptide binding cleft are valuable reagents for identifying T cells that bind specific peptide-MHC complexes. Two studies in this week's issue show that disulfide-stabilized (DS) MHC class I molecules offer a more efficient path to preparing large libraries of MHC-peptide reagents. Saini *et al.* developed DS versions of three MHC class I molecules and used a library of DS HLA-A2–peptide multimers to rapidly screen T cells infiltrating human melanoma tumors for neoantigen reactivity. Moritz *et al.* prepared libraries of DS HLA-A2–peptide complexes to screen an affinity-matured TCR for cross-reactivity with self-peptide–MHC complexes. Empty MHC class I molecules that are stable and easily loaded with peptide will facilitate the wider use of MHC-peptide reagents for T cell detection. See related Research Article by Saini *et al.* in this issue.

View the article online
https://www.science.org/doi/10.1126/sciimmunol.aav0860
Permissions
https://www.science.org/help/reprints-and-permissions

Use of this article is subject to the Terms of service